Biochemical and Biophysical Research Communications 416 (2011) 140–145

Contents lists available at SciVerse ScienceDirect

Biochemical and Biophysical Research Communications

journal homepage: www.elsevier.com/locate/ybbrc

Structure and dimerization of translation initiation factor aIF5B in solution

Louise Carøe Vohlander Rasmussen [a], Cristiano Luis Pinto Oliveira [b,1], Olwyn Byron [c], Janni Mosgaard Jensen [a], Jan Skov Pedersen [b], Hans Uffe Sperling-Petersen [a], Kim Kusk Mortensen [a,*]

[a] Department of Molecular Biology, Aarhus University, Gustav Wieds Vej 10, DK-8000 Aarhus C, Denmark
[b] Department of Chemistry, Centre for mRNP Biogenesis and Metabolism, and iNANO Interdisciplinary Nanoscience Center, Aarhus University, Langelandsgade 140, DK-8000 Aarhus C, Denmark
[c] Glasgow Biomedical Research Center, University of Glasgow, Glasgow G12 8QQ, Scotland, United Kingdom

ARTICLE INFO

Article history:
Received 19 October 2011
Available online 11 November 2011

Keywords:
Archaeal translation initiation factor aIF5B
Structure determination
Dimerization
Small-angle X-ray scattering
Analytical ultracentrifugation

ABSTRACT

Translation initiation factor 5B (IF5B) is required for initiation of protein synthesis. The solution structure of archaeal IF5B (aIF5B) was analysed by small-angle X-ray scattering (SAXS) and dynamic light scattering (DLS) and was indicated to be in both monomeric and dimeric form. Sedimentation equilibrium (SE) analytical ultracentrifugation (AUC) of aIF5B indicated that aIF5B forms irreversible dimers in solution but only to a maximum of 5.0–6.8% dimer. Sedimentation velocity (SV) AUC at higher speed also indicated the presence of two species, and the sedimentation coefficients $s^0_{20,w}$ were determined to be 3.64 and 5.51 ± 0.29 S for monomer and dimer, respectively. The atomic resolution (crystallographic) structure of aIF5B (Roll-Mecak et al. [6]) was used to model monomer and dimer, and theoretical sedimentation coefficients for these models were computed (3.89 and 5.63 S, respectively) in good agreement with the sedimentation coefficients obtained from SV analysis. Thus, the structure of aIF5B in solution must be very similar to the atomic resolution structure of aIF5B.

SAXS data were acquired in the same buffer with the addition of 2% glycerol to inhibit dimerization, and the resultant monomeric aIF5B in solution did indeed adopt a structure very similar to the one reported earlier for the protein in crystalline form. The $p(r)$ function indicated an elongated conformation supported by a radius of gyration of 37.5 ± 0.2 Å and a maximum dimension of ~130 Å. The effects of glycerol on the formation of dimers are discussed.

This new model of aIF5B in solution shows that there are universal structural differences between aIF5B and the homologous protein IF2 from *Escherichia coli*.

1. Introduction

In Archaea, initiation of translation is a process that incorporates both bacterial and eukaryotic features. The archaeal mRNAs resemble bacterial ones, inasmuch as they are uncapped and include Shine–Dalgarno-like (SD-like) sequences [1]. Start codon recognition is consequently based on SD/anti-SD interaction [2]. On the other hand, the archaeal initiation factors share features with eukaryotic homologues. This is exemplified by the fact that the Met-tRNA$_i$ is brought to the ribosome as a ternary complex by aIF2, a homologue of eukaryotic eIF2 [3,4]. Furthermore, aIF5B is thought to stimulate ribosomal subunit joining in a manner similar to its eukaryotic counterpart eIF5B [5]. However, the exact mechanism of translation initiation in Archaea is still unknown.

Structural investigations of archaeal initiation factors have shed light on the functions of the eukaryotic counterparts. In the case of aIF5B, the crystal structure for this protein [6], being the only full-length atomic resolution structure of this initiation factor, has also been used to model bacterial IF2 in different ribosomal complexes [7], sometimes requiring domain rearrangements for satisfactory fits [8,9]. However, the structure of the C-terminal part of IF2 in solution has been shown by small-angle X-ray scattering (SAXS) studies to be markedly different from the crystal structure of aIF5B [10]. Furthermore, bacterial IF2 contains an additional N-terminal part comprising three domains, which are not present in the archaeal homologue and can therefore not be accounted for by the aIF5B crystal structure.

In order to determine whether aIF5B adopts the same structure in solution as in the solid crystal, or whether it has a structure similar to the solution structure of homologous IF2, aIF5B was

Abbreviations: aIF5B, archaeal translation initiation factor 5B; AUC, analytical ultracentrifugation; DLS, dynamic light scattering; IF, translation initiation factor; SAXS, small-angle X-ray scattering; SE, sedimentation equilibrium; SV, sedimentation velocity.

* Corresponding author. Fax: +45 86182812.
E-mail address: kkm@science.au.dk (K.K. Mortensen).
[1] Present address: Institute of Physics, University of São Paulo, Rua do Matão, Travessa R 187, Cidade Universitária, São Paulo, Brazil.

0006-291X/$ - see front matter © 2011 Elsevier Inc. All rights reserved.
doi:10.1016/j.bbrc.2011.11.012

analysed by SAXS and dynamic light scattering (DLS). Comparing the data with the crystal structure revealed an equilibrium between monomers and dimers. Sedimentation equilibrium (SE) and sedimentation velocity (SV) analytical ultracentrifugation (AUC) was used to analyse this dimerization further. A second SAXS analysis of aIF5B in the same buffer with 2% glycerol showed no dimerization, and a model for aIF5B in solution was generated.

2. Materials and methods

2.1. Protein expression and purification

The expression vector pGEX-6P-1[GST-aIF5B] was a kind gift from Dr. Thomas E. Dever. Due to the presence of rare codons in the *infB* gene encoding aIF5B, the vector was transformed into Rosetta(DE3)[pLysS-R.A.R.E.] cells for protein expression. The cells were incubated in 2xTY medium at 37 °C with constant shaking, and recombinant protein expression was induced by addition of IPTG to a final concentration of 0.1 mM. The cells were harvested and broken by sonication. The GST fusion protein was purified by affinity chromatography (elution using 10 mM reduced glutathione). The eluted protein was dialysed in 1 L PreScission Protease cleavage buffer and then cleaved with PreScission Protease (GE Healthcare). The GST-tag was removed by affinity chromatography. The aIF5B protein was further purified by hydrophobic interaction chromatography on a HiTrap Phenyl HP column (GE Healthcare, elution by decreasing salt gradient) and concentrated using ion exchange chromatography (Q FF column, GE Healthcare, elution by increasing salt gradient) and Vivaspin ultrafiltration columns (GE Healthcare). Finally, the protein was dialysed in SAXS buffer (20 mM TrisHCl pH 7.6, 100 mM NaCl, 1 mM $MgCl_2$, 0.1 mM PMSF, 1 mM DTT). The protein concentration was determined by measuring the absorbance at 280 nm using a NanoDrop 2000 spectrophotometer (Thermo Fisher Scientific).

2.2. Small-angle X-ray scattering (SAXS)

SAXS data were recorded first with a laboratory-based SAXS instrument [11] in the Chemistry Department of Aarhus University. Two concentrations were measured (0.6 and 1 mg/mL) in order to account for possible particle aggregation and other concentration effects. Data reduction was performed using home-written software. The SAXS-intensity is recorded as a function of the momentum transfer modulus q ($q = 4\pi\sin(\theta)/\lambda$, where λ is the radiation wavelength and 2θ is the scattering angle). Pure water was used as primary standard for absolute scale normalization [11]. SAXS data were also recorded at the Advanced Photon Source (APS) at the Argonne National Laboratory in Chicago. Three concentrations were measured (0.6, 0.9 and 1.2 mg/mL), and data reduction was performed using IGOR Pro [12]. Measurements of cytochrome c scattering data were used for absolute scale normalization. The SAXS data were analysed using data analysis software from the ATSAS program suite: Data scaling and merging was performed in PRIMUS [13]. Indirect Fourier transformation resulting in the characteristic real-space distance distribution function $p(r)$ was performed using GNOM [14]. GASBOR [15,16] was used for *ab initio* modelling, and model alignment and averaging was performed using SUBCOMP [17] and DAMAVER [16]. Calculation of theoretical solution SAXS intensity curves from atomic coordinates of protein structure and comparison with experimental data was performed using CRYSOL [18]. The estimation of the polydispersity and oligomeric population was obtained by the program OLIGOMER [19]. Model visualization and generation of figures was done using the program PyMol [20].

2.3. Dynamic light scattering

DLS data were recorded at 0.6 mg/mL aIF5B using a light scattering instrument from ALV (Langen, Germany), which is a CGS-8F goniometer system equipped with an ALV-6010/EPP multi-tau digital correlator and a helium–neon diode laser (JDS Uniphase). Data measurements were performed at 90°. The software provided with the system was used for deriving the hydrodynamic (Stokes) radius using cumulant analysis and CONTIN method [21]. The Stokes radius is related to the diffusion of a particle in a certain liquid and is a function of the temperature and the fluid characteristics (the Stokes–Einstein equation for a sphere in a liquid is $D = k_BT/6\pi\eta R_{Stokes}$, where D is the translational diffusion constant, k_B is the Boltzmann constant, T is the temperature, η is the liquid viscosity and R_{Stokes} is the Stokes radius).

2.4. Analytical ultracentrifugation (AUC)

AUC experiments were performed on a Beckman Coulter Optima XL-I analytical ultracentrifuge (Beckman Coulter, Palo Alto, CA, USA) with an An-50 Ti 8-hole rotor, 12 mm path-length charcoal-filled epon double-sector centrepieces and interference optics. The experiments were carried out at 4 °C in SAXS buffer. Laser delay was adjusted prior to the runs to obtain high-quality interference fringes. Sedimentation velocity (SV) experiments were performed at a rotor speed of 49,000 rpm using 360 µl samples of aIF5B at seven different concentrations (0.1, 0.3, 0.6, 0.9, 1.2, 1.5 and 2 mg/mL). A series of 480 scans at 1 min intervals was obtained for each sample. The data were analysed using size-distribution $c(s)$ analyses in SEDFIT v11.71 software [22,23]. Buffer density (ρ = 1.00482 g/mL) and viscosity (η = 0.015912 Poise) at 4 °C were calculated from the buffer composition and the partial specific volume of aIF5B at 4 °C (0.739 mL/g) was calculated from the amino acid sequence using SEDNTERP software [24]. A molecular mass of 66,661 Da was calculated from the amino acid sequence. Sedimentation equilibrium (SE) data were acquired for 80 µl of the same seven aIF5B samples at 4 °C at two different rotor speeds (15,000 and 17,000 rpm). After 30 h at 17,000 rpm 10 scans were obtained at 3 h intervals until equilibrium was ascertained using WinMATCH (www.biotech.uconn.edu/auf/?i=aufftp) software. The rotor was decelerated to 15,000 rpm, and 10 further scans were obtained, also at 3 h intervals until a second equilibrium was attained. The SE data were fitted using SEDPHAT v6.21 software [25,26].

3. Results and discussion

3.1. SAXS and DLS analysis

The aIF5B protein was expressed as a GST fusion protein in BL21(DE3) Rosetta and purified by affinity column chromatography. The GST tag was removed by proteolytic cleavage, and aIF5B was purified by affinity, hydrophobic interaction and ion exchange chromatography. Following buffer change to SAXS buffer, aIF5B was analysed using SAXS.

Since the experimental data were normalized to an absolute scale, the forward scattering from aIF5B can be used to calculate the molecular weight for aIF5B, which was found to be ~95 kDa. Since the expected molecular weight is 66.7 kDa, this suggested the presence of both monomers and dimers.

To determine the agreement of the measured SAXS data with the crystal structure of aIF5B, CRYSOL was used to compute the theoretical SAXS intensities of the crystal structure based on the atomic coordinates and compare these with the experimentally obtained SAXS data. As observed in Fig. 1, fitting the experimental

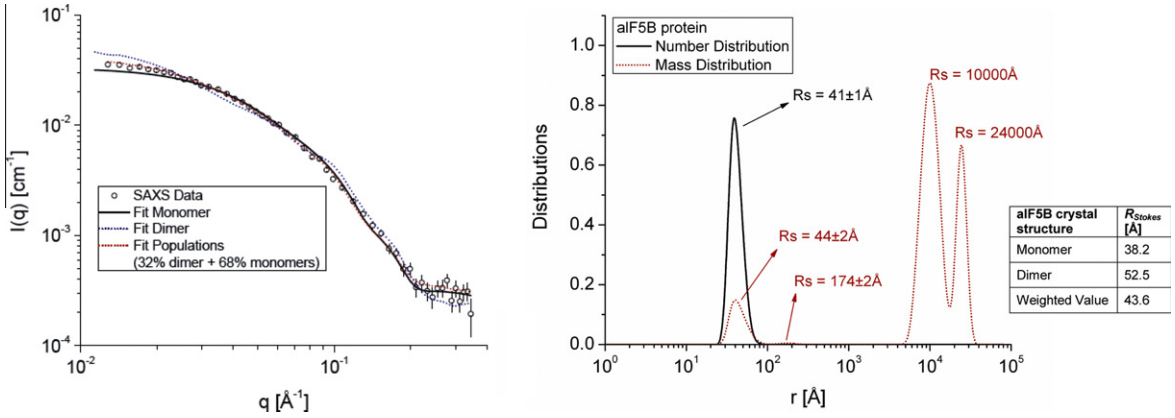

Fig. 1. SAXS and DLS data. Left: Scattering intensity of aIF5B is depicted as a function of the momentum transfer modulus q. The SAXS data indicate a population of 68% monomers and 32% dimers. Right: The DLS data give both a number and a mass distribution as shown here. The table shows the R_{Stokes} values of the aIF5B crystal structure for comparison to the DLS data.

SAXS data to the monomeric crystal structure data did not give a satisfactory result, and neither did the fitting to a dimeric crystal structure. From the analysis assuming a polydisperse system, the best fit of the experimental SAXS data was to a population of 68% monomers and 32% dimers of the crystal structure, the weight average of which agrees with the molecular weight experimentally determined by SAXS.

The DLS data also support the presence of dimers. These data give the distribution of sizes according to a given radius and result in both a number distribution and a mass distribution (Fig. 1). In the case of a number distribution, calculations are performed assuming that the distribution of sizes is a histogram of the number of particles. In a mass distribution, a factor R^3 is included as a weight for the distribution and therefore more weight will be given to particles with larger sizes, and sizes that could not be seen in the number distribution due to low concentration might appear. As seen in Fig. 1, the peak at ~41 Å becomes more asymmetric in the mass distribution, compared with the number distribution, and another contribution appears at ~174 Å along with small fractions of very large aggregates of more than 10,000 Å. This technique does not have the resolution to resolve monomers and dimers, but the fact that the ~41 Å peak is not very sharp and a little asymmetric and that the asymmetry increased when changing the weight, indicates that both monomers and dimers are present in solution. Furthermore, the measured R_{Stokes} is larger than that calculated from the crystal structure, whereas the averaged value (weighted by the proportions obtained from the polydisperse fit to the SAXS data) is very close to the one obtained experimentally.

3.2. AUC

To establish the presence of the monomer–dimer equilibrium, AUC was performed. Sedimentation velocity (SV) experiments are used to observe the entire time-course of sedimentation and report on the size distribution of the solubilised macromolecules as well as reversible chemical equilibria. The SV data were initially analysed using size distribution $c(s)$ analysis [27] with SEDFIT v11.71 software. The data (every 5th scan of the 480 originally acquired) were fitted with a resolution in sedimentation coefficient-space of 200 over the range 0.0–6.0 S (at 4 °C). The $c(s)$ overlay is dominated by single peaks (Fig. 2) at $s_{20,w} \approx 3.7$ S with evidence of minor peaks at low sedimentation coefficient (s), probably arising from buffer components, and high s (a small amount of aggregate) but importantly a reproducible minor peak at $s_{20,w} \approx 5.4$ S. In order to rigorously determine the sedimentation coefficients of these two species, the data were fit with the non-interacting discrete

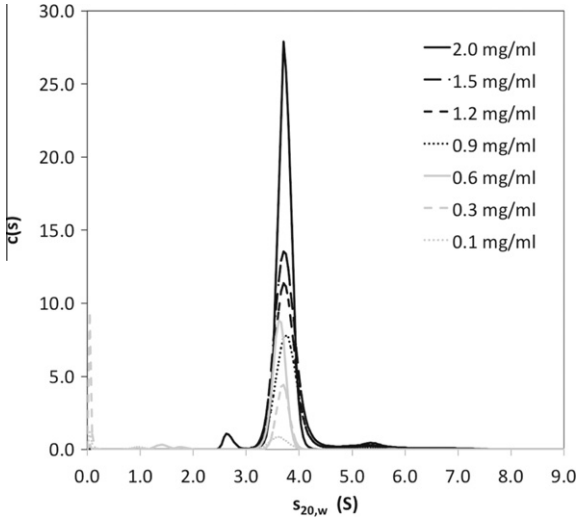

Fig. 2. SV analysis of aIF5B. $c(s)$ distributions (standardised to water at 20 °C) derived via SEDFIT from SV interference data collected over a range of sample concentrations.

species model in SEDFIT that employs finite-element analysis. For the dominant species the resultant sedimentation coefficients were then corrected to standard conditions of temperature and solvent before being extrapolated to infinite dilution to obtain a sedimentation coefficient independent of concentration $s^0_{20,w} = 3.64$ S. The minor species (at most 5%) was returned only for the fits to the higher concentration data (1.2, 1.5 and 2.0 mg/mL) and therefore it was not valid to undertake linear regression to obtain $s^0_{20,w}$. Instead the range of values (5.21–5.78 S) and their average 5.51 ± 0.29 S will be used for further analysis.

The sedimentation coefficient was computed for the aIF5B crystal structure. The PDB file 1G7R (PDB ID: 1G7R) containing the atomic coordinates for aIF5B is an incomplete structure. The missing residues were modelled using the protein structure prediction server I-TASSER [28], which returned a structure identical to 1G7R apart from the missing loops, which were successfully included in the model. The resultant coordinates were submitted to the SOMO module of the UltraScan II program [29,30] to generate a realistically hydrated hydrodynamic bead model, and the sedimentation coefficient was computed to be 3.89 S. This is in reasonable agreement with the experimentally obtained value of 3.64 S. The experimental value may be slightly lower than that computed as the

result of moderate molecular flexibility. The sedimentation coefficient was computed using SOMO for a dimer model constructed from the I-TASSER monomer. This gave a value of 5.63 S, consistent with the average $s_{20,w}$ determined experimentally for the putative dimeric species.

The SE data were fitted using SEDPHAT v6.21 software. Firstly the data were individually fitted using the Species Analysis approach. When one species was used, molecular masses significantly higher (typically ≈73 kDa) than the known monomer mass (66.6 kDa) were obtained. Therefore the data (acquired at 15 k and 17 k rpm) were globally fitted with two models: a two-species model and a monomer–dimer model. In both models, the monomer mass was fixed at 66.6 kDa. The two-species model returned a mass of 134.1 kDa for the second species, which was 6.8% of the sample (with a reduced χ^2 value of 8.86), whereas the monomer–dimer model returned a K_d of 708 μM (with a reduced χ^2 value of 31.15). The two-species model provides a better fit to the SE data than the monomer–dimer model, indicating that aIF5B forms irreversible dimers in solution (Fig. 3). The results of the SE analysis are consistent with the SV data: both detect a maximum of 5–6.8% dimer, neither indicates reversible equilibrium between monomer and dimer.

There is a notable difference in the dimer estimates using AUC (5–6.8%) and SAXS (32%). This disagreement indicates that dimer formation depends on sample concentration and sample environment. The SAXS data may be affected by a very small amount of aggregate (observed in DLS), which skew the amount of dimer in the model. The AUC data is not affected by formation of aggregates, since aggregates are removed from the system by the centrifugal field. This may explain the difference in dimer estimation.

3.3. SAXS analysis in 2% glycerol

When the scattering intensity of aIF5B in SAXS buffer was measured at the APS synchrotron, some radiation damage was observed. A common way of avoiding this is adding a small amount of glycerol to the samples. Indeed, adding only 2% glycerol to the aIF5B samples prevented the occurrence of radiation damage, and as an added bonus the data now indicated only monomeric protein. These data gave a molecular weight of 63.9 ± 3.7 Å in line with the expected molecular weight of monomeric aIF5B of 66.7 kDa. The best data (acquired at the two highest concentrations) were processed in PRIMUS, scaled according to concentration and merged. The features of the original data sets were preserved, and the merged data were used for further analysis.

The monodispersity of the sample was confirmed by the Guinier plot (Ln[$I(q)$] versus q^2), which showed very good linearity (Fig. 4A). This plot also gave a radius of gyration R_g of 36.6 ± 0.4 Å, which agrees well with the R_g of 37.5 ± 0.2 Å obtained from indirect Fourier transformation by GNOM. The maximum dimension was estimated to be 130 Å indicating an elongated protein shape, which is also shown by the skewed appearance of the distance distribution function $p(r)$ (Fig. 4B). Comparison of the monodisperse SAXS data for aIF5B with the scattering curve computed from the crystal structure with CRYSOL shows a very high similarity at low angles but small differences at high angles (Fig. 4C, for this fit an additional constant background was optimized).

GASBOR was used to generate an *ab initio* model for aIF5B from the SAXS data and the amino acid sequence of aIF5B. GASBOR uses a chain of dummy residues to model the protein backbone, and through a simulated annealing approach this chain is arranged in a shape fitting the SAXS data. The low resolution of SAXS prevents the generation of one unique model, so 20 repeats were performed, and the ten models of lowest χ^2 were averaged using DAMAVER. The best representative of all generated models (lowest χ^2) is shown in cyan superimposed onto the average in grey (Fig. 4D). There is very good agreement between the best *ab initio* model and the average, which indicates that this *ab initio* model is a good

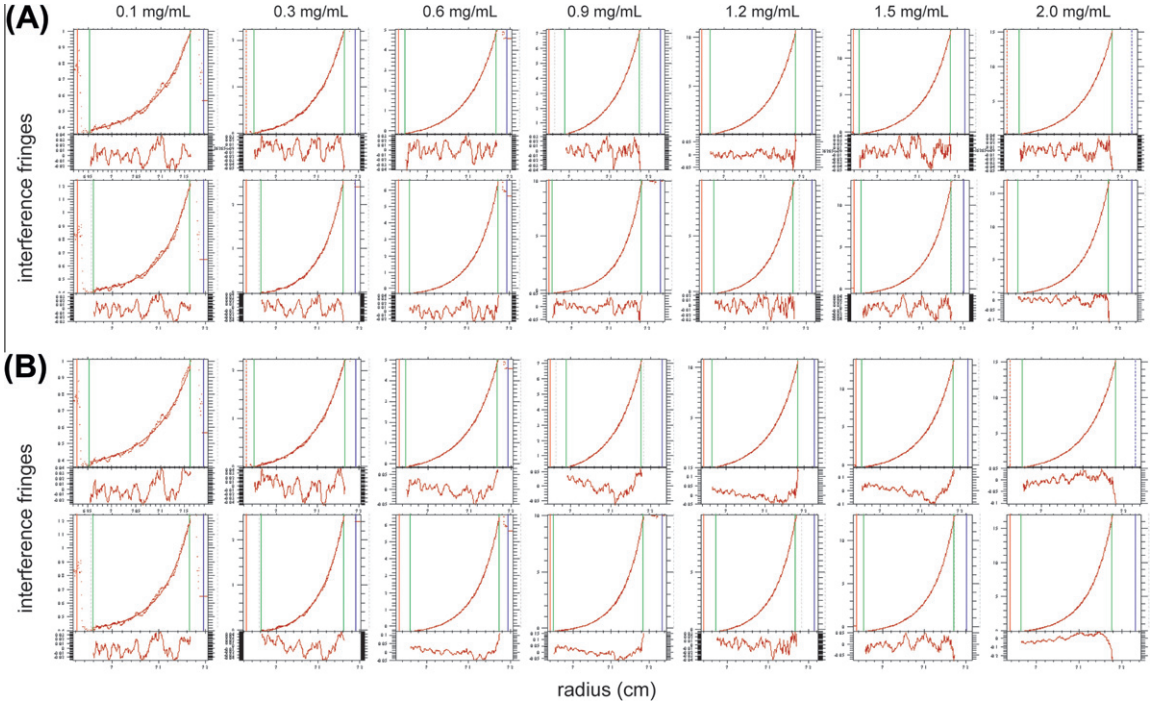

Fig. 3. SE analysis of aIF5B. Best global fits (smooth lines) to the SE interference data (dotted lines) using (A) a two-species model and (B) a monomer–dimer model in SEDPHAT. In each of (A) and (B) the upper row depicts data acquired at 15 k rpm, whilst the data in the lower row were acquired at 17 k rpm. The loading concentrations are indicated above the uppermost row. Residual plots are shown beneath each fit. The two-species model returned a mass of 134.1 kDa for the second species (6.8% of the sample) (reduced χ^2 = 8.86), whereas the monomer–dimer model returned a K_d of 708 μM (reduced χ^2 = 31.15).

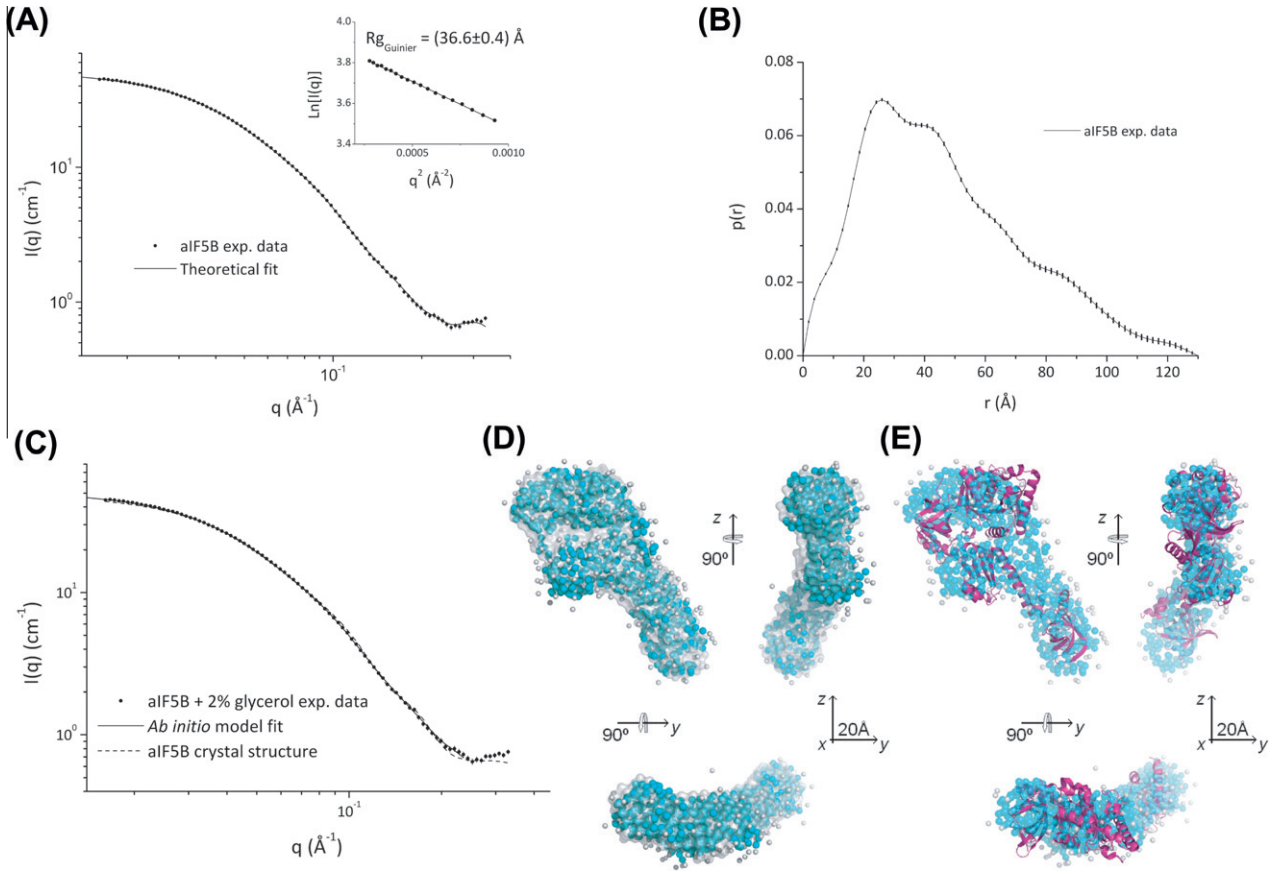

Fig. 4. SAXS analysis of aIF5B in 2% glycerol. (A) Scattering intensity is depicted as a function of the momentum transfer modulus *q*. The theoretical fit to the SAXS data was generated with GNOM, and the insert shows a Guinier plot with a significant region of linearity. (B) Indirect Fourier transformation with GNOM gave a skewed distance distribution function *p*(*r*). (C) SAXS data for monodisperse aIF5B compared with the scattering intensity computed for the aIF5B crystal structure and the best *ab initio* model. (D) The best *ab initio* model (cyan) is superimposed onto an average of the ten best models (grey) and shown in three perpendicular orientations. The small grey spheres are dummy water molecules simulating the hydration shell. (E) The crystal structure of aIF5B (magenta) is superimposed onto the best *ab initio* model (cyan). The small grey spheres are dummy water molecules simulating the hydration shell. (For interpretation of the references to colour in this figure legend, the reader is referred to the web version of this article.)

representation of the SAXS data. This is also clear from Fig. 4C, where the *ab initio* model is fitted to the aIF5B scattering intensity data.

SUPCOMB was used to compare the best *ab initio* model with the crystal structure, and the two structures are very alike (Fig. 4E). This establishes that aIF5B has the same structure in crystal and soluble phase and that aIF5B and *Escherichia coli* IF2 are indeed distinct structures, irrespective of the state of the protein (crystal form or soluble) and the applied analysis.

The dimer formation of aIF5B was affected by the addition of glycerol. Glycerol is widely used as a protein stabilizer. It reduces the number of available water molecules and therefore protein conformational freedom, thereby increasing stability. At high concentrations of glycerol and protein, dimerization has been observed to be enhanced [31]. This seems to involve the formation of strong non-covalent interactions between protein and glycerol and close contact between monomers, resulting in protein oligomers adducted with glycerol [32]. Here both glycerol and protein concentration is lower. The dimer formation in the absence of glycerol may be caused by a slight instability of the monomer, causing it to form small amounts of dimer. Addition of just a small amount of glycerol stabilizes the protein and prevents dimerization. Adding larger amounts of glycerol, maybe accompanied by higher protein concentration, would probably drive the equilibrium towards dimers or even higher oligomerization.

Acknowledgments

The authors thank Liang Guo from the Argonne National Laboratory in Chicago for his help with SAXS measurements and data treatment.

This research was supported by Danish Natural Science Research Council Grants 21-03-0592 and 21-03-0465 and by Carlsberg Grants 2005-1-126, 2006-1-167 (to H.U.S.-P. and K.K.M.) and 2007-1-261 (to L.C.V.R.).

References

[1] S.D. Bell, S.P. Jackson, Transcription and translation in Archaea: a mosaic of eukaryal and bacterial features, Trends. Microbiol. 6 (1998) 222–228.
[2] P.P. Dennis, Ancient ciphers: translation in Archaea, Cell 89 (1997) 1007–1010.
[3] N. Pedulla, R. Palermo, D. Hasenohrl, U. Blasi, P. Cammarano, P. Londei, The archaeal eIF2 homologue: functional properties of an ancient translation initiation factor, Nucleic Acids Res. 33 (2005) 1804–1812.
[4] L. Yatime, E. Schmitt, S. Blanquet, Y. Mechulam, Functional molecular mapping of archaeal translation initiation factor 2, J. Biol. Chem. 279 (2004) 15984–15993.
[5] J.H. Lee, S.K. Choi, A. Roll-Mecak, S.K. Burley, T.E. Dever, Universal conservation in translation initiation revealed by human and archaeal homologs of bacterial translation initiation factor IF2, Proc. Natl. Acad. Sci. USA 96 (1999) 4342–4347.
[6] A. Roll-Mecak, C. Cao, T.E. Dever, S.K. Burley, X-Ray structures of the universal translation initiation factor IF2/eIF5B: conformational changes on GDP and GTP binding, Cell 103 (2000) 781–792.

[7] A.G. Myasnikov, S. Marzi, A. Simonetti, A.M. Giuliodori, C.O. Gualerzi, G. Yusupova, M. Yusupov, B.P. Klaholz, Conformational transition of initiation factor 2 from the GTP- to GDP-bound state visualized on the ribosome, Nat. Struct. Mol. Biol. 12 (2005) 1145–1149.
[8] G.S. Allen, A. Zavialov, R. Gursky, M. Ehrenberg, J. Frank, The cryo-EM structure of a translation initiation complex from *Escherichia coli*, Cell 121 (2005) 703–712.
[9] A. Simonetti, S. Marzi, A.G. Myasnikov, A. Fabbretti, M. Yusupov, C.O. Gualerzi, B.P. Klaholz, Structure of the 30S translation initiation complex, Nature 455 (2008) 416–420.
[10] L.C. Rasmussen, C.L. Oliveira, J.M. Jensen, J.S. Pedersen, H.U. Sperling-Petersen, K.K. Mortensen, Solution structure of C-terminal *Escherichia coli* translation initiation factor IF2 by small-angle X-ray scattering, Biochemistry 47 (2008) 5590–5598.
[11] J.S. Pedersen, A flux- and background-optimized version of the NanoSTAR small-angle X-ray scattering camera for solution scattering, J. Appl. Cryst. (2004) 369–380.
[12] IGOR Pro by WaveMetrics, www.wavemetrics.com, last accessed 2011-10-07.
[13] P.V. Konarev, V.V. Volkov, A.V. Sokolova, M.H.J. Koch, D.I. Svergun, Primus - a Windows-PC based system for small-angle scattering data analysis, J. Appl. Cryst. 36 (2003) 1277–1282.
[14] V. Semenyuk, D.I. Svergun, GNOM - a program package for small-angle scattering data-processing, J. Appl. Cryst. 24 (1991) 537–540.
[15] D.I. Svergun, M.H.J. Koch, Small-angle scattering studies of biological macromolecules in solution, Rep. Prog. Phys. 66 (2003) 1735–1782.
[16] V.V. Volkov, D.I. Svergun, Uniqueness of *ab-initio* shape determination in small-angle scattering, J. Appl. Cryst. 36 (2003) 860–864.
[17] M.B. Kozin, D.I. Svergun, Automated matching of high- and low-resolution structural models, J. Appl. Cryst. 34 (2001) 33–41.
[18] D.I. Svergun, C. Barberato, M.H.J. Koch, CRYSOL - a program to evaluate X-ray solution scattering of biological macromolecules from atomic coordinates, J. Appl. Cryst. 128 (1995) 768–773.
[19] A. Sokolova, V.V. Volkov, D.I. Svergun, OLIGOMER program, www.embl-hamburg.de/biosaxs/manual_oligomer.html, last accessed 2011-10-07.
[20] The PyMOL Molecular Graphics System, version 0.99, by Schrödinger LLC, New York, www.schrodinger.com/products/14/25/, last accessed 2011-10-07.
[21] S.W. Provencher, CONTIN: A general purpose constrained regularization program for inverting noisy linear algebraic and integral equations, Comput. Phys. Commun. 27 (1982) 229–242.
[22] SEDFIT, www.analyticalultracentrifugation.com/download.htm, last accessed 2011-10-07.
[23] P. Schuck, Size-distribution analysis of macromolecules by sedimentation velocity ultracentrifugation and lamm equation modeling, Biophys. J. 78 (2000) 1606–1619.
[24] J. Philo, D. Hayes, T. Laue, SEDNTERP, www.jphilo.mailway.com/download.htm, last accessed 2011-10-07.
[25] SEDPHAT, www.analyticalultracentrifugation.com/sedphat/download.htm, last accessed 2011-10-07.
[26] P. Schuck, On the analysis of protein self-association by sedimentation velocity analytical ultracentrifugation, Anal. Biochem. 320 (2003) 104–124.
[27] P. Schuck, M.A. Perugini, N.R. Gonzales, G.J. Howlett, D. Schubert, Size-distribution analysis of proteins by analytical ultracentrifugation: strategies and application to model systems, Biophys. J. 82 (2002) 1096–1111.
[28] A. Roy, A. Kucukural, Y. Zhang, I-TASSER: a unified platform for automated protein structure and function prediction, Nature Protocols 5 (2010) 725–738.
[29] N. Rai, M. Nöllmann, B. Spotorno, G. Tassara, O. Byron, M. Rocco, *SOMO* (*SO*lution *MO*deler): differences between x-ray and NMR-derived bead models suggest a role for side chain flexibility in protein hydrodynamics, Structure 13 (2005) 723–734.
[30] E. Brookes, B. Demeler, C. Rosano, M. Rocco, The implementation of SOMO (SOlution MOdeller) in the UltraScan analytical ultracentrifugation data analysis suite: enhanced capabilities allow the reliable hydrodynamic modeling of virtually any kind of biomacromolecule, European Biophys. J. Biophys. Lett. 39 (2010) 423–435.
[31] P.L. Darke, J.L. Cole, L. Waxman, D.L. Hall, M.K. Sardana, L.C. Kuo, Active human cytomegalovirus protease is a dimer, J. Biol. Chem. 271 (1996) 7445–7449.
[32] M.A. Mendes, B.M. de Souza, L.D. dos Santos, K.S. Santos, M.S. Palma, Analyzing glycerol-mediated protein oligomerization by electrospray ionization mass spectrometry, Rapid. Commun. Mass. Spectrom. 19 (2005) 2636–2642.